EEET ECOLOGICAL ENGINEERING & ENVIRONMENTAL TECHNOLOGY

Ecological Engineering & Environmental Technology, 2026, 27(7), 251–269
https://doi.org/10.12912/27197050/222333
ISSN 2719–7050, License CC-BY 4.0

Received: 2026.05.13
Accepted: 2026.06.15
Published: 2026.07.01

Mechanically reinforced ultraporous aluminum-iron pillared bentonite-silicon carbide ceramic membranes for sustainable dye filtration

Sisnayati[1*], Muhammad Azmi[1], Dewi Putri Yuniarti[1], Ria Komala[1], Dian Sari Dewi[1], Surya Hatina[1], Kiagus Ahmad Roni[2]

[1] Department of Chemical Engineering, Faculty of Engineering, Universitas Tamansiswa Palembang, Jl. Tamansiswa No. 500, Kepandean Baru, Ilir Timur I, Palembang 30126, South Sumatra, Indonesia
[2] Department of Chemical Engineering, Faculty of Engineering, Universitas Muhammadiyah Palembang, Jl. Jend. Ahmad Yani, 13 Ulu, Seberang Ulu II, Palembang 30263, South Sumatra, Indonesia
* Corresponding author's e-mail: sisnayati@unitaspalembang.ac.id

ABSTRACT

This work was focused on synthesizing mechanically reinforced ultraporous ceramic membranes derived from Al–Fe pillared bentonite and silicon carbide for sustainable dye filtration along with investigating the relationship among composition, microstructure, porosity, mechanical strength, permeate flux and methylene blue rejection. Preparation of Al–Fe pillared bentonite involves thermal activation, templated intercalation using the Al–Fe polycation, filtration, drying and calcination. Composite membranes were prepared by mixing Al–Fe pillared bentonite with SiC in mass ratios of 100:0, 80:20, 60:40, 40:60, 20:80 and 0:100 and subsequently pressing at a pressure of 50 kg/cm^2 for one minute, drying for 48 h and sintering at a temperature of up to 800 °C for a period of 10 h. Membrane morphology and pore structure measurements were determined from SEM image analysisand the filtration characteristics were evaluatedat1.6 bar through the use of methylene blue as amodel dye pollutant. The porosity ranged between 46.83–52.44% and the mean pore sizes varied from 0.12–0.28 μm. The highest flexural strength of these membranes was 28.6 MPa obtained for a 40:60 Al-Fe pillared bentonite/SiC membrane which meant that each prepared porous ceramic shaped body showed better structure integrity respect to unpilled membranes. All the determined membranes demonstrated high dye rejection (≥ 83%) values, while in comparison to pure pillared bentonite membrane, the SiC-contained membranes provided a more stable flux behavior and better rejection performance. However, the porosity was derived primarily using SEM image analysis, so validating it with traditional void and surface characterization techniques will be necessary. The proposed membranes provide a promising low-cost, energy-efficient textile wastewater treatment in practice. Originality of this work consists in combining adsorption-active Al–Fe pillared bentonite with SiC material which could add to the structural strength ensuring a compromise between pore size distribution, dye rejection and mechanical stability.

Keywords: ultraporous ceramic membrane, pillared bentonite, silicon carbide, dye filtration, mechanical strength.

INTRODUCTION

The increasing need for clean water has led to the occurrence of more advanced technologies in order to filter out persistent organic pollution from effluent streams, especially synthetic dyes from textile wastewater. This is particularly true for the coagulation as traditional methods of treatment which cannot completely remove persistent dyes such as methylene blue (MB), due to their high solubility (Akash et al., 2024; do Carmo et al., 2024; Marques et al., 2025), complex aromatic structures (Ramteke et al., 2025), poor biodegradability (Malebadi et al., 2025). These methods however have considerable limitations and membranes based separation technologies have appeared as a promising type of method due to its high efficiency (Jarrar et al., 2024), processing simplicity

(Akoumeh et al., 2025), and eco-friendliness (Elshazly and Fahmy, 2025; Rakcho et al., 2025). Nevertheless, the high cost of fabrication and service lifetime for commercial membranes are still main obstacles for their large-scale application.

In order to overcome disadvantages, Low Cost Ceramic Membrane (LCCMs) based on natural minerals and industrial waste materials have been paid great attentions. Aluminosilicate clay such as bentonite is an attractive natural raw material for economic production of ceramics material due its high plasticity (Chihi et al., 2024; Rakcho et al., 2025; Satyannarayana et al., 2022), chemical resistance (Foorginezhad et al., 2023), and ion exchange properties (Saja et al., 2020). However, natural bentonite's inherent mesoporosity and mechanical fragility preclude its use in high flux filtration systems (Boutaleb et al., 2024). Intercalation with metal polycations, particularly Al^{3+} and Fe^{3+}, has shown to be effective method for interlayer and mesoporous framework formation with improve surface area, thermal stability, and catalytic performance (Biswas and Majumder, 2026; Parodia et al., 2021). The investigations proved that Al Fe-pillared bentonite having better thermal stability and structural strength can be used as candidate of composite ceramic matrix (Desai et al., 2023; Kanth et al., 2025).

Si-C doped clay-based membranes have also shown to provide excellent mechanical strength (do Carmo et al., 2024)(Boutaleb et al., 2024), chemical resistance (Marques et al., 2025) and hydrophilicity along with high porosity and permeability (Bahrouni et al., 2025). Although SiC ceramics possess excellent resistance to harsh conditions, their sintering temperature (above 1300 °C) is relatively high for direct uses. Thus, the integration of SiC with pillared bentonite would have a synergistic effect to obtain dual-functionality, superior mechanical durability given by SiC and high adsorption-filtration function endowed by Al-Fe pillared bentonite (Abdel-Azim et al., 2025; Rezala et al., 2020). Hybrid composite of negative index ceramic components have shown enhanced functional ability in terms of dye removal efficiency, mechanical strengths when SiC is incorporated with clay-based matrices (Boutaleb et al., 2025)(Bahrouni et al., 2025). However, systematic studies that focus on optimization of Al-Fe pillars cascade into ultraporous SiC framework to induce dual filtration-adsorption attributes are still very rare.

The treatment of dye-contaminated wastewater via ceramic membranes impacts both academic and industrial fields, despite the availability of low-cost options. However, some scientific gaps have not yet been solved. Recent studies investigated clay-based ceramic membranes as promising low-cost filtration materials, while SiC-containing ceramic advanced membranes boast higher mechanical strength and chemical resistance, pore stability, antifouling performance (Boutaleb et al., 2024; Akash et al., 2024; Jarrar et al., 2024; do Carmo et al., 2024; Marques et al., 2025). Nevertheless, most of the previous studies addressed them individually as permeability booster, adsorption augment or mechanical fortifier in a synergistic way. The challenge of combining adsorption-active Al-Fe pillared bentonite and structurally reinforcing SiC in a single ultraporous ceramic membrane system has not been addressed systematically to date. In particular, how the Al-Fe pillared bentonite/SiC composition affects pore evolution, pore size distribution as well as mechanical strength, permeate flux and methylene blue rejection has not been fully investigated. Understanding this knowledge gap is important because the performance of ceramic membranes is not only dictated by total porosity, but also by the interplay between pore connectivity, surface adsorption sites, phase distribution and mechanical integrity.

Thus the current investigation seeks to formulate mechanically enhanced ultraporous ceramic membranes possessing higher strength related features by incorporating pillared bentonite (Al-Fe) and SiC for green dye filtration. Most importantly, the original scientific justification of this study is to improve knowledge regarding composition-microstructure-performance behavior of Al-Fe pillared bentonite/SiC ceramic membranes and understand the role of SiC fraction towards porosity, pore size distribution, mechanical strength, permeate stability and methylene blue rejection. The working hypothesis is that an appropriate Al-Fe pillared bentonite /SiC ratio will yield a porous structure with good characteristics for water permeability, great mechanical performance and high dye rejection at the same time.

MATERIALS AND METHODS

Materials

The major precursor for the ceramic membranes was natural bentonite clay (purchased from

a local chemical supplier in Palembang, Indonesia). A commercial silicon carbide (SiC) powder with purity ≥99% and average particle size of 1–5 µm (Sigma-Aldrich, USA) was used as reinforcing and pore-forming component. The pillaring solution was prepared by using aluminium nitrate nonahydrate [$Al(NO_3)_3 \cdot 9H_2O$, analytical grade, Merck, Germany], iron (III) nitrate nonahydrate [$Fe(NO_3)_3 \cdot 9H_2O$, analytical grade, Merck, Germany] and sodium hydroxide (NaOH, ≥98%, Merck Germany). All experimental procedures were performed with the use of de-ionized water. Methylene blue (MB, analytical grade; Merck, Germany) was chosen to be a model dye pollutant for the membrane filtration tests. The textile wastewater was directly collected from a traditional jumputan textiles industry Tiga Putri Bahar, Jumputan Fabric Center, Tuan Kentang Village, Jakabaring District, Palembang, Indonesia., to present practical textile wastewater conditions.

Preparation of Al–Fe pillaring solution

The Al–Fe pillaring solution was synthesized using a slightly modified hydrolysis-intercalation method. First, 60 g of $Al(NO_3)_3 \cdot 9H_2O$ was dissolved in 320 mL deionized water to prepare a solution of Al^{3+}, and then, 32.32 g $Fe(NO_3)_3 \cdot 9H_2O$ was dissolved in 160 mL deionized water to obtain the same concentration of Fe^{3+} (0.5 M). The Al/Fe molar ratio was kept constant at 2:1. Then 19.2 g NaOH was dissolved in 960 mL deionized water for a preparation of 0.5 M NaOH solution. The mixed Al–Fe nitrate solution was stirred at 500 rpm, and NaOH solution was added dropwise for controlled hydrolysis. Hydrolysis was performed at pH 4.0–4.5 to prevent metal hydroxides from prematurely precipitating. The suspension was aged for 24 h at room temperature (25-30°C) to encourage the formation of stable Al–Fe polyhydroxyl cations. The bentonite-to-pillaring solution ratio is kept at 1:5 (w/v).

Preparation of Al–Fe pillared bentonite

In order to eliminate moisture and enhance interlayer accessibility, raw bentonite was thermally activated at 400 °C for 2 h using a programmable muffle furnace (heating rate 5 °C/min). Then, the activated bentonite was slowly added into the Al–Fe pillaring solution while continuously stirring at a speed of 500 rpm for 24 h. The suspension was then filtered through Whatman No. 42 filter paper and dried overnight at room temperature (20 °C) for 24 h, after which the resulting solid was calcined at 400 °C for 2 h in order to convert the intercalated polycations into stable oxide pillars of varying length. Whereafter, the calcined substance was grinded in an agate mortar, and then sieved with 100-mesh sieve to prepare Al–Fe pillared bentonite powder uniformly.

Fabrication of ultraporous ceramic membranes

Al–Fe pillared bentonite (AFPB) and SiC powder were mixed at various weight ratios, such as A (100:0), B (80:20), C (60:40), D (40:60), E (20:80) and F(0:100) to fabricate the ceramic membranes. The formulation of 20 g of mixed powder was blended with 15 mL deionized water to form a doughy plastic paste. The shaped paste was pressed into flat-disc membranes in a stainless-steel mold with a 50 mm diameter and target thickness of 4 ± 0.2 mm. A hydraulic press was used for uniaxial pressing at 50 kg/cm^2 for a period of 30 min. Membrane specimens had an average green body weight of 18 ± 0.5 g and all formulations were produced in triplicate for repeatability.

The green membranes were dried for 48 h at room temperature and then put into an oven at 105 °C overnight (12 h) and sintered in a programmable furnace under atmospheric conditions at 800 °C for 10 h by heating with speed of 3 °C/min to the target temperature followed by cooling to room temperature with a rate of 2 °C/min. The ultraporous structure can be maintained compared to the high temperature process, but also the energy consumption is lower, which drove the selection of low-temperature sintering strategy. This new membrane formation mechanism was that Al–Fe oxide pillars were intercalated into bentonite interlayers for improved adsorptive functionality while SiC particles served as microporous rigid reinforcing domains and pore-stabilizing agents, leading to the development of complex interconnected bicontinuous pore networks during thermal treatment.

Membrane characterization

The ceramic membranes were investigated by using scanning electron microscopy (SEM) to determine the surface morphology and pore structure, energy-dispersive X-ray spectroscopy (EDS) to verify elemental distribution, X-ray diffraction

(XRD) to identify crystalline phase and mechanical testing to determine membrane strength. The sintered membrane samples were sectioned into pieces representative of the thickness, mounted on SEM stubs before analysis. SEM images were taken at various magnifications in order to inspect surface morphology, particle arrangement, pore distribution, pore connectivity and potential defects within the structure of membranes.

SEM micrographs based on ImageJ and Origin estimation of pore size and apparent surface porosity. These SEM images were converted to grayscale images and underwent threshold segmentation on the grayscale image to separate pore areas from that of the solid ceramic matrix. Apparent Surface Porosity which was calculated as follows:

$$\text{Apparent surface porosity (\%)} = (A_p / A_t) \times 100 \quad (1)$$

where: A_p is the total pore area and A_t is the total analyzed image area. The pore size distribution derived from the pore diameters measured and processed with Origin software to calculate frequency distribution curves.

Since SEM image analysis is an analysis of two-dimensional surface features, the resulting porosity values were taken to be those of image based apparent porosity rather than (exc) absolute total porosities. Open porosity shall be validated according to Archimedes water immersion method in order to improve reliability.

$$\text{Open porosity (\%)} = [(W_s - W_d)/(W_s - W_{sub})] \times 100 \quad (2)$$

where: W_d is the dry membrane weight, W_s is the air-dry saturated membrane weight and W_{sub} is the saturated membrane weight when fully immersed in water. This forms the basis of validation, since it is well known that open porosity and pore connectivity are key determining factors regarding flux, fouling behavior and dye rejection.

Filtration performance evaluation

A laboratory-scale membrane filtration unit comprising a feed tank, pump, pressure-control valve, pressure gauge and membrane housing was used to assess microfiltration (MF) performance. Under constant pressure of 1.6 bar, the feed solution was pumped through the membrane installed inside the housing. The filtration test time was 60 min. Prior to filtration, the membrane was prewetted with distilled water to degas the pores and equilibrate water transport.

For flux studies, the permeate volume was collected at defined time intervals during filtration. Methylene blue solution was chosen as the model dye pollutant, whereas real jumputan textile wastewater was used to simulate actual textile wastewater conditions. The permeate flux was calculated as:

$$J = V / (A \times t) \quad (3)$$

where: J is permeate flux (L/m^2.h), V is permeate volume (L), **A** is effective membrane area (m^2) and t filtration time (h).

Dye rejection analysis

Dye rejection was evaluated by determining the absorbance of feed and permeate samples with a UV-Vis spectrophotometer. The blank for the measurement was made using distilled water. The absorbance was measured at λmax of methylene blue, where 4 mL sample was placed in a clean cuvette. Typically the maximal absorbance wave length for methylene blue solution is at about 664 nm but this must be experimentally confirmed by scanning the dye solution before analysis.

The percentage dye rejection was calculated using the following formula:

$$R\ (\%) = [(C_0 - C_t)/C_0] \times 100 \quad (4)$$

where: R is the rejection efficiency of the dye, C_0 is the initial concentration in feed and C_t is the concentration of dye present in permeate at filtration time t. Since absorbance is proportional to the dye concentration according to Beer-Lambert relationship, rejection can also be calculated using absorbance values as follows:

$$R\ (\%) = [(A_0 - A_t)/A_0] \times 100 \quad (5)$$

where: A_0 and A_t are the initial absorbance of feed solution and absorbance of permeate, respectively. Absorbance readings should be taken in triplicate, and results expressed as mean ± standard deviation.

All steps of membrane preparation were proposed in order to save energy as much as possible by using moderate sintering temperature and naturally occurred raw materials. The pillared bentonite-SiC composite was designed for

the fabrication of a dual-function membrane as it combined mechanical reinforcement and adsorption–filtration properties for sustainable wastewater treatment. The research flowchart is presented in Figure 1.

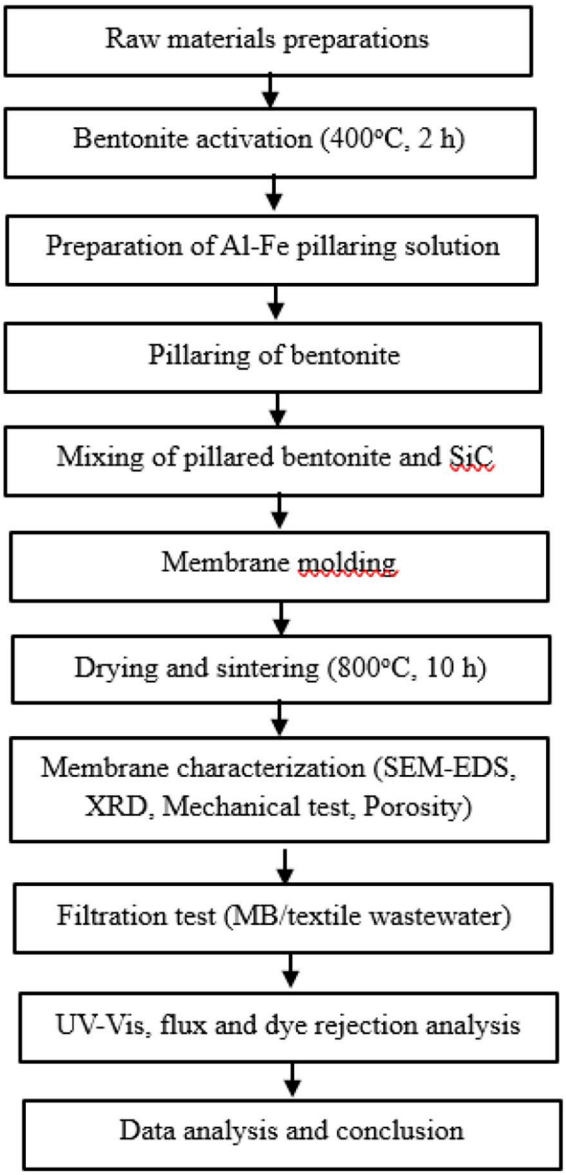

Figure 1. Flowchart of Al-Fe pillared bentonite-SiC ceramic membrane preparation and application

RESULTS AND DISCUSSION

Morphological characterization of Al-Fe pillared bentonite-SiC membranes

The surface morphology of the Al–Fe pillared bentonite–SiC ceramic membranes with various compositions (A–F) was analysed by scanning electron microscopy (SEM) at 10.000X magnification, as displayed in Figure 2 (a-f). SEM specimens were sampled from sintered flat-disc membranes that were manufactured mixing Al-Fe pillared bentonite (AFPB) and SiC into a past, which was applied at 50 kg/cm^2 for 30 min, green bodies were air-dried for 48 h and then sintered at 800 °C for the duration of 10 h. Small fragments representative of the membranes in content, namely through central regions from where they were cut, cleared from free particles after extraction out (Kilic et al., 2021b), fixed onto stubs for SEM, structures observed visually assessed so as to contemplate pore distribution, main particle packing order or structural defectiveness. The SEM images clearly display that the microstructure of the membrane is significantly influenced by the relative content of pillared bentonite and silicon carbide (SiC), which leads to well-defined textural transformation from clay-dominated channels structure to SiC-enriched compact arrangement.

SEM specimens i.e. the samples for scanning electron microscopy were taken from the surface of sintered flat-disc ceramic membranes, which were prepared in the inverse proportions from Al–Fe pillared bentonite and SiC (samples A–F). Representative fragments from each sintered membrane were carefully cleaned to remove any loose particles, affixed onto aluminium stubs with conductive carbon tape and observed at 10.000X magnification (SEM). Membranes A–E were all as-sintered membranes visible as a rigid porous ceramic discs, while membrane F comprised solely of silica carbide. It was brittle and fragile when handled since no clay-based binder phase had formed.

The fabricated Al–Fe pillared bentonite–SiC ceramic membranes with different AFPB/SiC compositions are shown in Figure 3. All membrane at first were moulded followed by sintering to form flat disc-shaped specimens. The clear visual change associated with the SiC incorporation can be explained. The reddish brown colour of membrane A, which consisted solely of AFPB, appeared dwelled due to the clay-based and Al–Fe oxide-containing matrix. As can be seen from membranes B to E, where the SiC content increased stepwise, the color of a membrane turned from brown into greyish-brown which suggests that SiC particles were blended into the AFPB matrix. Membrane F, consisting of pure SiC (for lack of a better term), demonstrated the darkest grey to black colouration, verifying that

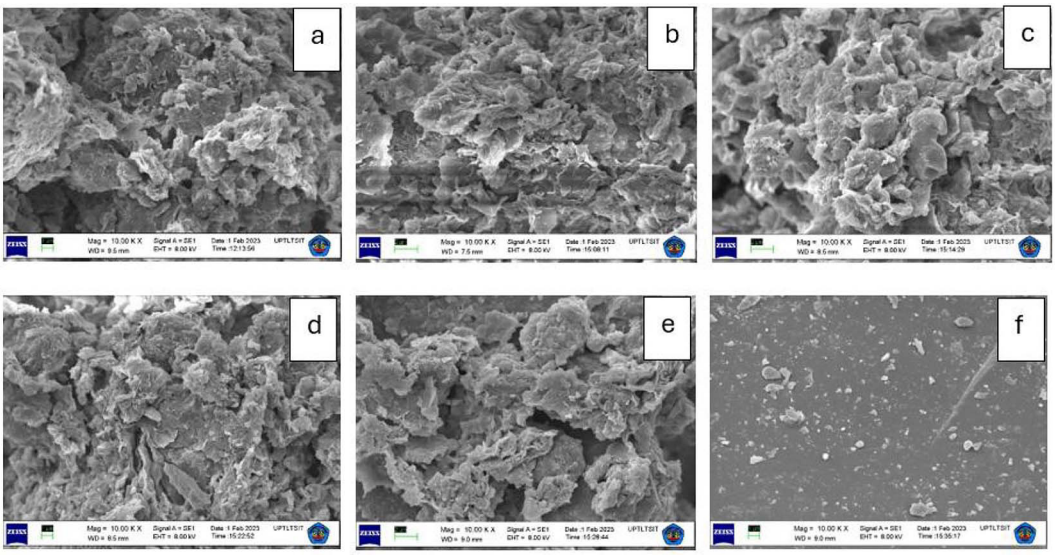

Figure 2. Surface morphology evolution of Al-Fe pillared bentonite-SiC ceramic membranes at different composition at 10.000X magnification. Membrane A = 100% AFPB; B = 80% AFPB/20% SiC; C = 60% AFPB/40% SiC; D = 40% AFPB/60% SiC; E = 20% AFPB/80% SiC; F = 100% SiC

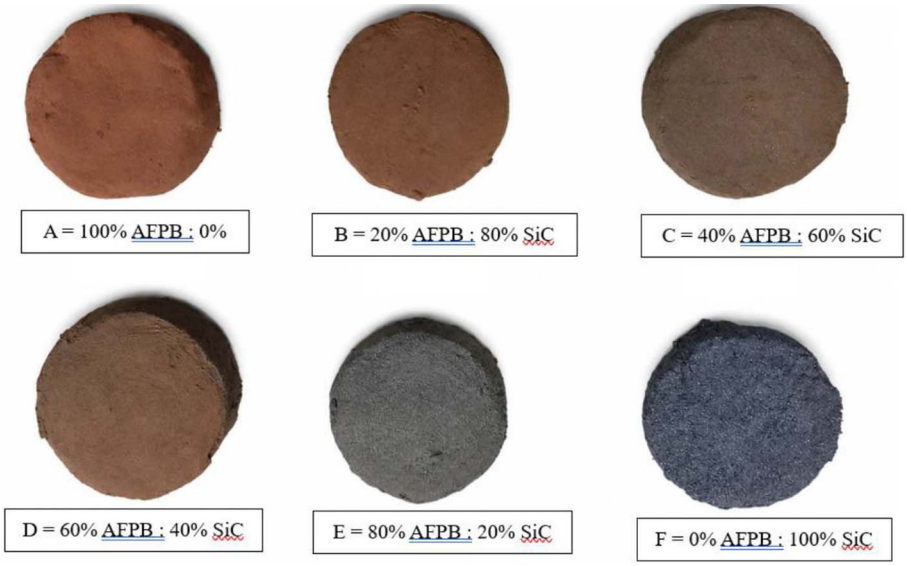

Figure 3. Membrane A = 100% AFPB; B = 80% AFPB/20% SiC; C = 60% AFPB/40% SiC; D = 40% AFPB/60% SiC; E = 20% AFPB/80% SiC; F = 100% SiC

indeed SiC is the dominant phase. Surface texture results also varied, with differences in color between modes. As a result, AFPB-rich membranes seemed clay-like and less dense, while those rich in SiC turned appeared dark through the more granular layer. These morphologic differences imply that the AFPB/SiC ratio had a significant effect on some of the general physical properties of the membranes prior to more detailed microstructural characterization. The ability to form disc-shaped membranes with a high success rate for all compositions indicates that AFPB could act as a ceramic matrix and binder, while SiC acts to modify the structure and reinforce it. The observed features in this preliminary visual inspection are consistent with further SEM analyses, which is expected to confirm alterations of pore structure, particle distribution and membrane compaction as a function of the AFPB and SiC relative weight.

The surface of membrane A (100% pillared bentonite, Figure 2(a)) is obviously very rough and heterogenous, comprising stacked or partially exfoliated clay platelets. There are many interparticle voids and irregular pore entrances,

which consist of a well-connected porous network. It is a type of morphology having fine average pore size, feature of Al–Fe pillared bentonite systems where metal oxide pillars stabilize the interlayer space and avoid structure collapse on sintering and conserve functional porosity (Ghohestani et al., 2022; Riyanti et al., 2024; Y. Wang et al., 2022). But a rigid ceramic reinforcement is lacking, hence the weak mechanical bonding force of clay.

Adding 20% (wt) SiC (membrane B, Figure 2(b)), the surface covers more compactly but presenting with open pore channels. SiC particles are found to be intertwined with the clay matrix, serving as skeleton support which connects the clay platelets and inhibits severe enlargement of pores. The synergistic effect increase the structural stability to be stronger, without degrading much pore connection which is essential for high permeate flux (Rakcho, Naboulsi, et al., 2024; J. Wang et al., 2024).

The microstructures of the membranes C (60% pillared bentonite–40% SiC) and D (40% pillared bentonite–60% SiC) (Figure 2 (c to d)) are the ones with more balance in all compositions. The SEM images indicate a bicontinuous porous structure comprising the interpenetrating microvoids between the clay-rich phase and SiC-modified skeleton. The pore channels become more homogeneous and continuous than those in A and B, without over-densification. The morphology indicated a good dispersion of SiC particles into the pillared bentonite matrix, enhancing mechanical reinforcement by load transfer while retaining adsorption-active surfaces of the clay. Such hybrid microstructures are recognized to provide a proper balance between permeability and mechanical stability in ceramic membranes (El-shazly and Fahmy, 2025; Marques et al., 2025). As a result of well-developed transport channels and stabilized pore walls, the membranes C and D are anticipated to have better flux–rejection performances. When SiC content was increased to 80 wt% (membrane E, Figure 2(e)), a much denser surface morphology can be observed. SiC aggregates were large and dominated the microstructure, whereas no continuous clay platelets can be observed. The pores are not fully removed, but their connectivity is notably diminished. Such densification is also related to the sensitivity and permeability, which however decreases in response to it (Liang et al., 2024; Wei et al., 2025).

In the most extreme case of membrane F (100% SiC, Figure 2(f)), it is noted that by SEM analysis the surface appears mainly smooth and dense with scarce visible pore channels. Pillared bentonite not being present, the binding and interlocking action given by the platelets of clay does not exist in this case and a weak intergranular strength among SiC particles was produced at the restricted sintering temperature (800 °C). Thus, membrane F was found to be very brittle and cracks/fractures easily during handling and testing. Such brittle behavior can be ascribed to the lack of forming sintering necks between SiC particles at an intermediate temperature (a common weak point of monolithic SiC ceramics without sintering aids or secondary binders) (Huang et al., 2023; Li et al., 2025). The lack of a ductile or laminated phase also compounds stress concentration, resulting in the weak mechanical strength of the membrane despite its obvious compactness. This finding accounts for the low membrane F worth in hydraulic-pressure-related filtration systems (do Carmo et al., 2024; Khmiri et al., 2023).

Over all, the SEM data confirm that the addition of Al–Fe pillared bentonite is essential for not only the generation of ultraporous structures but also improving their mechanical strength by platelet interlocking and stabilization using pillars (Achiou et al., 2025; El Abbadi et al., 2025). On the other hand, excessive SiC addition, in particular for membrane F gives dense but fragile structures with low fracture resistance. The dual presence of clay-originated porosity and SiC-caused reinforcement in C and D creates a reinforcing–porous composite structure, which enables high flux, efficient dye rejection and sufficient mechanical resistance (Hamad et al., 2024; Roy, 2025).

Energy-dispersive X-ray spectroscopy (EDS) elemental analysis

The EDS spectra of membranes A–F confirmed that the main elements forming Al–Fe pillared bentonite–SiC ceramic membranes (C, O, Al, Si, Fe) were present. On membrane A, O, Si and Al were the three most abundant elements, accounting for 47.9 wt. %, 23.1 wt. %, and 13.5 wt. wt %, and Fe concentration was 5.7 wt %. % and C at 7.0 wt. %. This implies that the matrix of membrane A was composed mainly from an aluminosilicate and Al–Fe oxide. C took over

as the dominant element in membrane B at 44.5 wt.%, followed by O 35.5 wt.%, Si 8.8 wt.%, Al 5.8 wt.%, and Fe 3.4 wt.%, indicating the presence of SiC-rich or carbon-bearing regions are contributing more.

Membrane C was more well-balanced in elemental composition, with O 42.0 wt.%, Si 18.8 wt.%, C 14.4 wt.%, Al 13.4 wt.%, and Fe 7.5 wt.%. This provides evidence for the simultaneous presence of aluminum silicate, Al–Fe oxide and silicon carbide phases. For membrane D, the highest was O on 48.1 wt. %, followed by Si 17.6 wt.%, C 15.4 wt.%, Al 11.9 wt.%, and Fe 4.9 wt.%. The presence of Al and Fe in all membranes demonstrates that Al–Fe pillared bentonite was incorporated into the membranes, while C and Si independently confirm that SiC was incorporated into the ceramic matrix.

For SiC-rich membranes, mainly E and F, the EDS spectra present stronger Si peaks in good agreement with their superior contribution from the forming of a SiC phase. Au peaks in membranes E and F were considered derived from a gold coating, used in SEM-EDS sample preparation, and as such not part of the membrane composition. Trace elements (Mg, K, Ca, Ti, S and Na) were also detected at the sub-ppmw level but are most likely related to mineral impurities in natural bentonite. All things considered, the EDS results are consistent with the formation of Al–Fe pillared bentonite–SiC composite ceramic membranes.

X-ray diffraction (XRD) analysis

Figure 5 shows the characteristics of the Al–Fe pillared bentonite–SiC ceramic membranes composition were highly dependent on XRD patterns as indicated by your following Figures: 9a to 9f respectively for membranes A-F. The broad background (15–35° 2θ) for all samples suggested the presence of amorphous or poorly crystalline aluminosilicate phases on pillared bentonite. The phenomenon is inherent for ceramic materials made from clay upon heat treatment.

Weak and broad diffraction peaks were obtained for membranes A-D, which could indicate that the ceramic matrix was mainly formed by pillared bentonite with low crystallinity. The diffractive characteristic peaks in the range of ~26–28° 2 θ were likely corresponding to silica/aluminosilicate-containing phases and a possible SiC contribution. Peaks became more pronounced and sharper with the addition of SiC, particularly in membranes E and F where it was clear that a higher crystalline contribution from the SiC phase occurred. Membrane E exhibited distinct peaks, especially at approximately 28°, 50°, 60–70° and higher than 75° at a value of 2θ along with this indicating an enhanced phase development and crystallinity compared to the bentonite-rich membranes.

The diffraction peaks attributed to the SiC framework were sharp for Membrane F as well, which contained the maximum SiC fraction

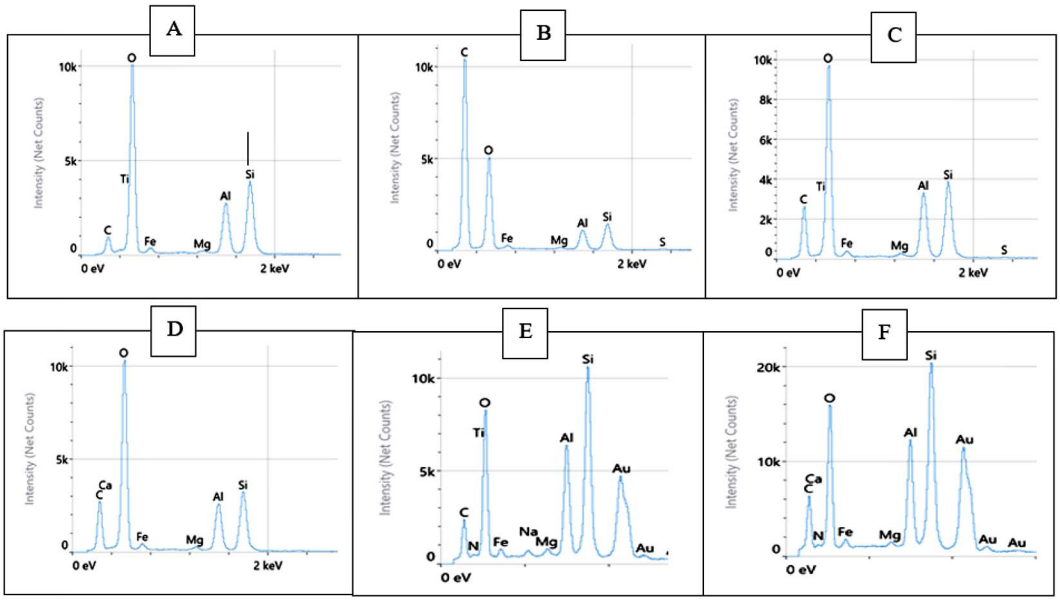

Figure 4. EDS spectra of ceramic membrane (A) 100% AFPB; (B) 80% AFPB : 20% SiC; (C) 60% AFPB : 40% SiC; (D) 40% AFPB : 60% SiC; (E) 20% AFPB : 80% SiC

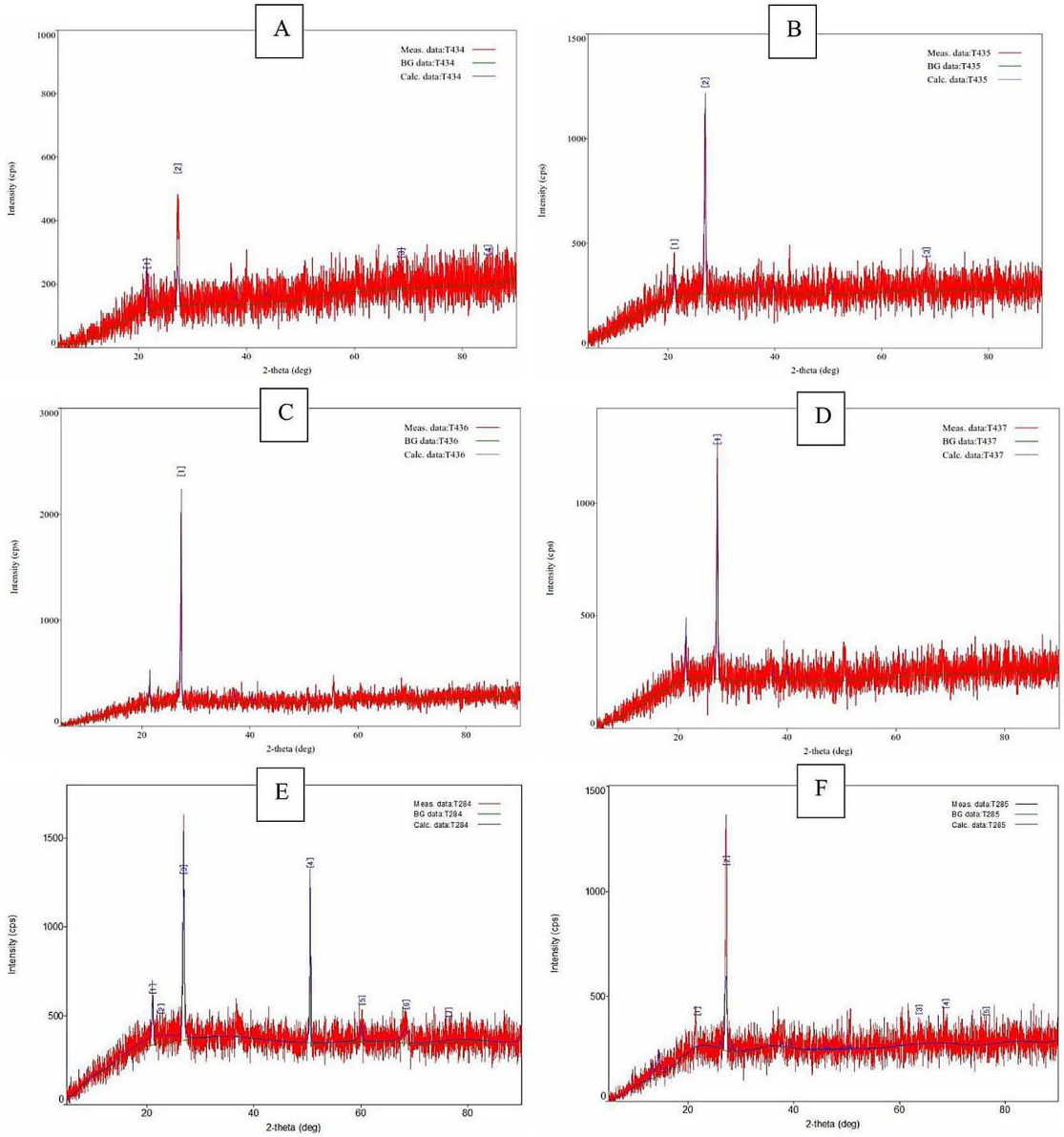

Figure 5. X-Ray diffraction patterns of AFPB-SiC ceramic membranes with different composisitions

during syndiotactic crystallization, confirming that crystalline SiC was indeed dominant in this case also. Nevertheless, the XRD background still remained noticeably broad, suggesting even after sintering at 800 °C some amorphous ceramic phases were retained and in general indicative of a mixed amorphous–crystalline structure within the membranes. Bentonite-rich membranes are mostly composed of amorphous aluminosilicate phases similar to fused silica, while increasing SiC content increases phase intensity for crystalline types. This strengthens the contribution of SiC to the structural ceramic and, likewise, verifies the successful manufacturing of Al–Fe pillared bentonite–SiC composite membranes.

Porosity

The relevant statistical parameters including average pore size, range of pores, number of pores as well as porosity were encapsulated in Table 1. The PSD relates it highly to membrane composition, and SiC is a factor in the double role of structurant and porogen agent for bentonite.

Values of porosity presented in Table 1 were first measured based on a apparent surface porosity calculated from several SEM micrographs and verified by the Archimedes water immersion method to provide higher confidence for the interpretation of porosity.

It used Origin software to find porosity in ceramic membrane pics of SEM. The porosity

of the silica-based ceramic membrane was then determined using the ratio between pore volume and total volumes of the ceramic membranes. Porosity quality was tested to determine the volume of material which can be absorbed into the silica-based ceramic membrane. By way of example, SEM image analysis can then help characterize the porosity of a sample ceramic membrane by using origin software. Then, the origin software will input SEM image and gives values that can be used to calculate porosity properties for each ceramic membrane. Origin Software was used to analyse the SEM images that produced the contour plot demonstrated in Figure 6.

The pore surface area of ceramic membranes is defined as the areas between the air cavities separated from solid unit (Figure 6). Origin software will know the volume of the matrix integral of the SEM image and additional data for porosity calculation can also be calculated using Excel Software. Table 1 show results of SEM image porosity analysis with origin software.

The 100 wt.% SiC (membrane F) was impossible to calculate quantitatively since SEM showed microcracks and broken particles and no clear open pores instead of a connected pore structure. This low mechanical strength hampers measurable PSD and porosity, highlighting pillared montmorillonite importance as a structural binder (Desai et al., 2023). The pure SiC without the clay matrix was incoherent and had isolated pores, as reported previously a ceramic binder phase is necessary for a stable porous membrane (Fu et al., 2025; Xue et al., 2023).

In this study, the Archimedes method of measuring open porosity using these three physical parameters was used to validate the porosity results obtained from SEM processing and ImageJ-OriginPro analysis. The calculation as:

$$\text{Open porosity (\%)} = [(W_s - W_d)/(W_s - W_{sub})] \times 100 \quad (6)$$

The calculated Archimedes values were nearly equivalent to the SEM-image porosity values

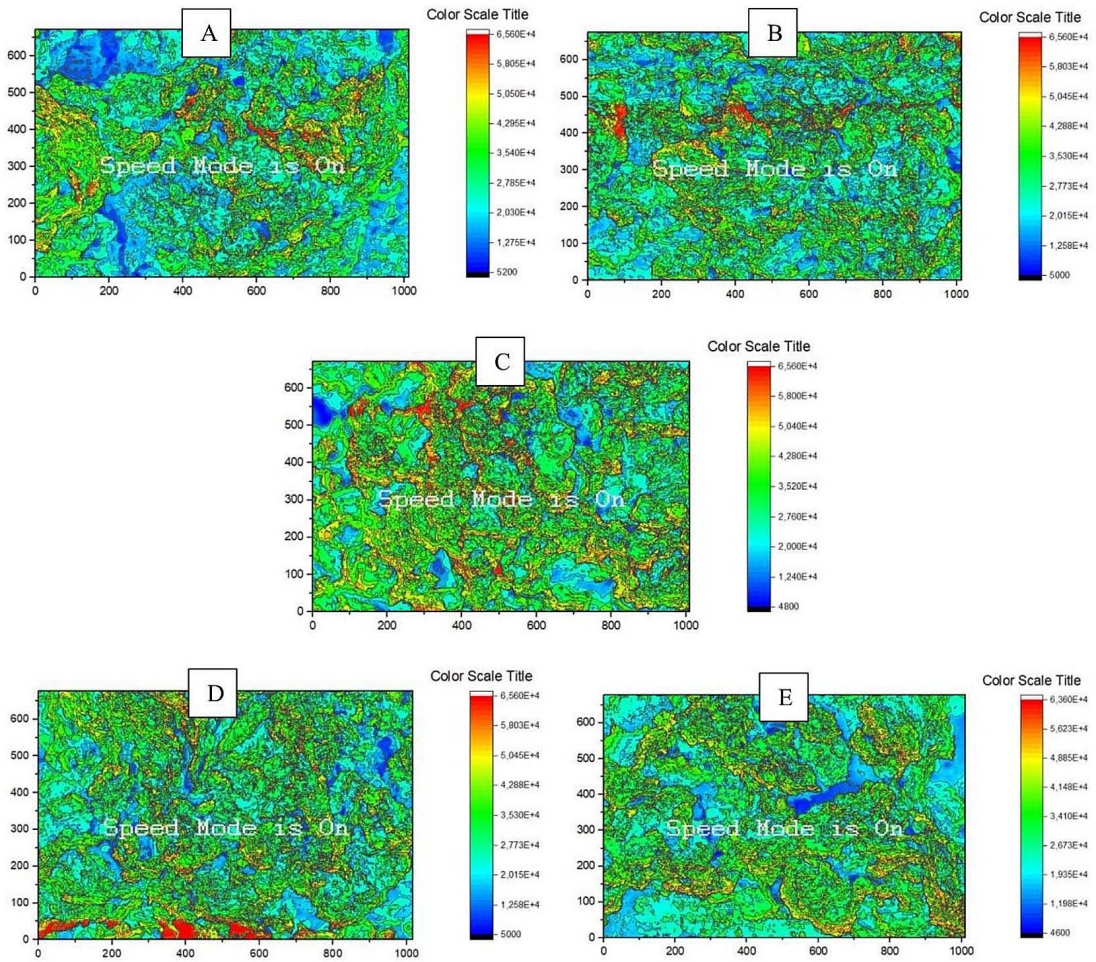

Figure 6. The SEM images of the ceramic membranes (A-E) after Origin Software analysis

Table 1. Porosity of ceramic membranes with varying Al-Fe pillared bentonite/SiC composition

Membranes	Composition pillared bentonite-SiC (wt%)	Number of pores (n)	Mean pore size (μm)	Range pore size (μm)	Porosity (%)	Remarks
A	100 : 0	182	0.14	0.05–0.30	52.44	Compact bentonite base structure
B	80 : 20	156	0.28	0.10–0.60	46.83	Highly open pore structure
C	60 : 40	164	0.22	0.08–0.45	48.49	Intermediate pore structure
D	40 : 60	176	0.12	0.06–0.25	50.79	Most compact structure
E	20 : 80	148	0.26	0.12–0.55	51.06	Open pore network dominated by SiC
F	0 : 100	-	-	-	-	Not measurable due to fragile structure

suggesting that image-based analysis of open pore structure is an adequate estimation.

Mechanical strength and microstructure model

The constituent features of the manufactured ceramic membranes were determined by porosity and flexural strength shown in Figure 7. No direct inverse linear correlation between the porosity and mechanical strength was seen in general. While increased pore volume commonly correlates with decreased strength in porous ceramics, the present data show that the structural arrangement of pores had a stronger influence than total porosity percentage alone.

Figure 7 shows at 50.79% porosity, membrane D has the highest flexural strength (28.6 MPa), indicating that its denser microstructure with a smaller average pore size would improve stress transfer and crack propagation resistance. Unlike the decreased porosity at membrane A corresponded with a increase in measurable strength (37.4 MPa), the actual strength however of membrane B was lowest amongst all three membranes (17.1 MPa) and also demonstrated no beneficial relationship between porosity (46.83%) nor pore size (86 μm) as open network structures with larger pores are far more damaging than measured stampable porosity alone (Rakcho et al., 2024; Yang et al., 2022). Membranes A and C exhibited intermediate performance between these, while membrane E showed low strength because of the high connectivity of open pores dominated by SiC. These results support increased efforts on controlling pore uniformity, pore connectivity and interparticle consolidation during sintering, in addition to just optimizing the overall porosity for ceramic membrane mechanics (Fu et al., 2024; Liang et al., 2024; Zhang et al., 2025).

The proposed microstructure evolution trend of Al–Fe pillared bentonite/SiC ceramic membranes based on composition ratio is shown in Figure 8. The schematic model to relate the porosity, pore size distribution and mechanical strength data yielding structural understanding of how the bentonite matrix and SiC filler collaboratively dictated membrane structure.

Figure 8 shows the distinct membrane performance being governed by a coupled approach

Table 2. Validation using Archimedes of open porosity of the samples, compared with porosity results generated by SEM-ImageJ-OriginPro

Membrane	AFPB:SiC (wt%)	Wd (g)	Ws (g)	Wsub (g)	SEM-ImageJ-OriginPro porosity (%)	Archimedes open porosity (%)	Difference (%)
A	100:0	8.120	12.250	4.350	52.44	52.28	0.16
B	80:20	8.350	12.020	4.150	46.83	46.63	0.20
C	60:40	8.480	12.290	4.430	48.49	48.47	0.02
D	40:60	8.620	12.590	4.780	50.79	50.83	0.04
E	20:80	8.750	12.730	4.920	51.06	50.96	0.10
F	0:100	-	-	-	-	-	Not measurable due to fragile structure

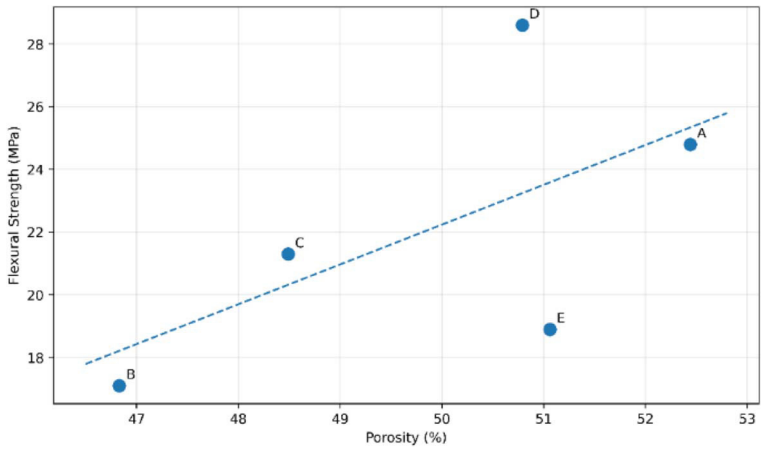

Figure 7. Relationship between porosity and mechanical strength of Al-Fe pillared bentonite/SiC ceramic membrane

to matrix continuity and rigid particle reinforcement. An insufficient reinforcement was produced at low SiC content whereas high SiC inclusion disrupted the cohesion of the matrix. Membrane D (40:60) showed the best composition through effective synergistic interaction of Al–Fe pillared bentonite and SiC, improving the microstructure leading to dense microstructures with fine pores providing higher mechanical stability (Fu et al., 2024; Hotza et al., 2020; Onyenanu and Nwabanne, 2025). This structural model follows previous workload similarities to the model porosity and strength results, who confirmed that pore morphology and particle packing played a greater role in the performance of such ceramic membranes than total porosity alone.

These results are especially important for membrane material development in filtration and wastewater treatment applications, where high permeability must be counterbalanced with

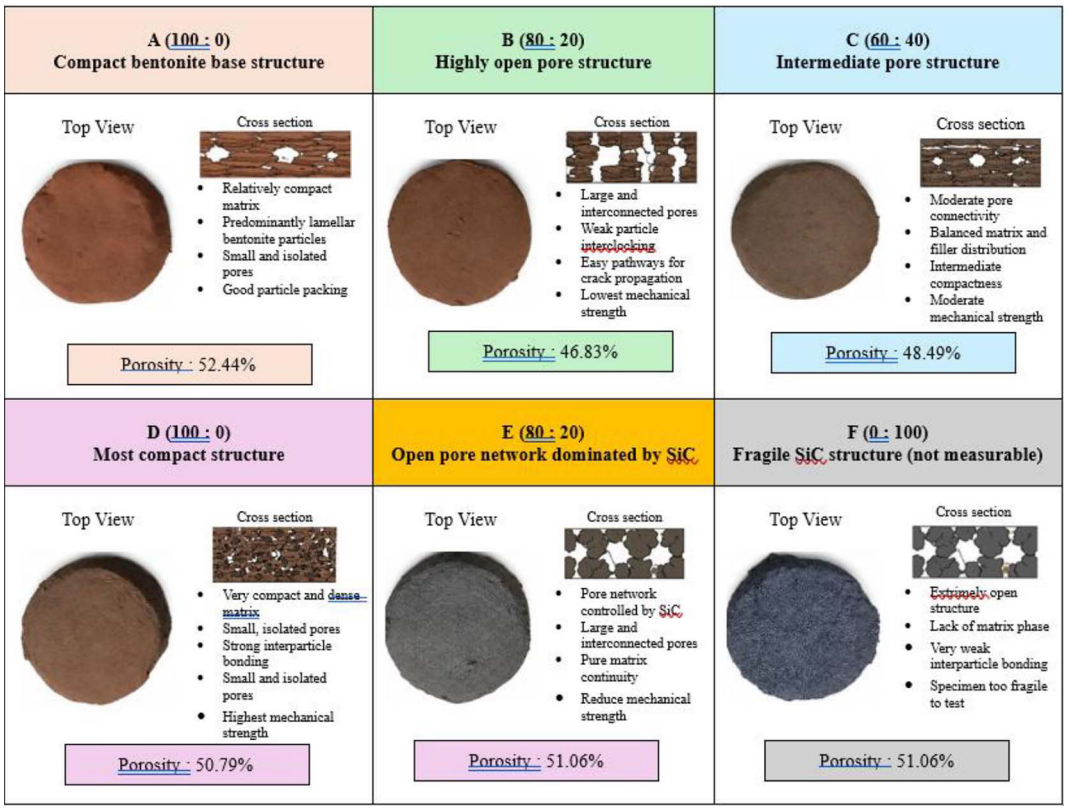

Figure 8. Schematic microstructure model of Al-Fe pillared bentonite/SiC ceramic membranes (A-F)

appropriate mechanical robustness. Hence, controlling both phase composition and microstructural packing is a pivotal route for the production of durable low-cost ceramic membranes from clay-based raw materials.

Permeat flux performance

The evolution of permeate flux for the ceramic membranes A–E constructed by a variety of proportions of Al–Fe pillared bentonite (AFPB) and SiC was compared as illustrated in Figure 8.

Figure 9 shows in all cases, membranes presented the typical sharp drop in flux during the first minutes of filtration (10–20 min), and then a slower decrease and stabilization after 30 minutes related to initial pore blocking by flocs and the boundary region period as new retention mechanisms seemed to have effective. Porous ceramic membranes frequently experience this form of fouling which is due to fast deposition of suspsended particles and solutes on the surface and inter-pore walls in the early stages of filtration (Cai et al., 2023; Xie et al., 2025).

At the start of filtration (10 min), membrane A containing 100 wt% AFPB displayed an initial flux of 1256 L/m².h which indicates a relatively open pore structure at a macroscopic scale. This membrane, however, still received the most severe flux reduction going down to 420 L/m².h at 20 min and even lower to only 16 L/m².h after an hour. The significant reduction of flux is indicative of severe pore blocking and cake layer formation that are presumably due to relatively smaller pore size distribution and higher fouling susceptibility compared to SiC based membranes (Jang et al., 2024; Sheng et al., 2025; Yan et al., 2025).

By comparison, the SiC-containing membranes (B–E) had lower initial fluxes than membrane A, but they showed better long-term stability. After 10 minutes, the starting flux was in the range of 796–866 L/m².h being a bit lower for membranes B–E, which suggested that the incorporation of SiC reduced slightly but not considerably the initial permeability caused by modification in pore structure and tortuosity (Ke et al., 2025). However, these membranes exhibited higher flux stability over time, in comparison with membrane A, indicating that SiC also conferred resistances to fouling resistance and physical strength (better anti-fouling property and structural stability) (Chen et al., 2022; Shi et al., 2023; Yan et al., 2025).

The sample D (40:60 AFPB/SiC) of the SiC-modified membranes demonstrated a relatively higher flux at 20 min (168 L/m².h) than that of membrane B, C, and E. This could be ascribed to its uniform but smaller pore size, which will help in achieving an optimal system between permeability and fouling resistance (Das et al., 2021). But after 30 min its flux stabilized to the other ones so that long term operation would be simply limited by surface fouling and not intrinsic membrane permeability (Liu et al., 2024; Onyenanu and Nwabanne, 2025). The equivalence in steady-state flux between the membranes (23–29 L/m².h after 60 min) B, D and E verifies that SiC addition may bring some similar resistance from

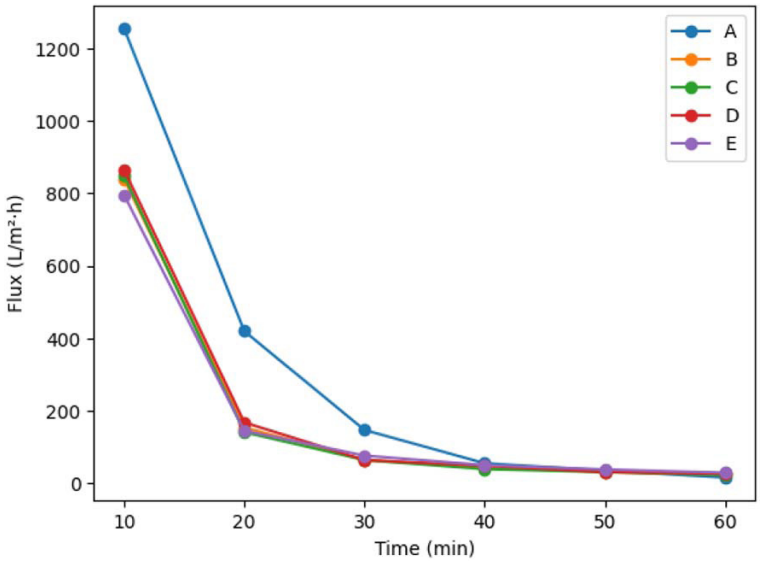

Figure 9. Variation of permeate flux with filtration time for ceramic membrane A–E

fouling while a stable cake layer formed (Wang et al., 2024; Zhu et al., 2022).

Although membrane A's porosity is higher, it fouled heavily because of its smaller pores and less stable structure. In contrast, membranes with SiC loadings of 20–80 wt% featured increased flux stability, which has been attributed to a tight SiC network that prevents collapsing of the pore and restricted movement of foulants causing irreversible fouling. This result is in line with previous reports indicating that ceramic additives like SiC can improve mechanical strength and reduce pore-crushing deformation during the filter operation (Fu et al., 2025).

In general the long-term performance of pure AFPB is lower than that of SiC-modified membranes, despite having higher initial flux. Membranes B (80:20) and E (20:80) demonstrate the most favorable tradeoff between initial flux and flux sustainability in the studied compositions and can be seen as suitable hopefuls for applicable operations requiring consistent separation performance.

Time-dependent rejection behavior

Figure 10 reveals the time-dependent rejection performance of ceramic membranes A–E via UV–Vis spectrophotometric analysis at an initial feed absorbance (A_0) of 1.656. All membranes showed high rejection factors during the entire filtration process (>83% Rejection), demonstrating good performance in separation. Nonetheless, rejection was found to decrease with time and upon modification of the membrane composition, indicating variations in pore size, fouling kinetic or surface–solute character.

Rejection efficiency at each filtration time was calculated directly from the measured UV–Vis absorbance of the feed and permeate solutions according to :

$$R(\%) = [(A_0 - A_t)/A_0] \times 100 \quad (7)$$

A_0 being initial feed absorbance (1.656) and A_t was permeate absorbance at a given filtration time, multiple determinations were obtained for all filtraion times to support the validity of rejection values.

The plotted rejection values were not hypothetical trends but actual absorbance data from the experiments. At the beginning of fouling (10 min), membrane A achieved a high level of rejection (93.96%), which can be attributed to its smaller average pore size (0.14 μm) and much denser microstructure thus enabling beneficial size exclusion mechanisms. In this case, low pore accessibility due to the clogging of the pores brings solute impedimen, which results in a common high rejection at such membranes with fine-pore clay-based structure (Malebadi et al., 2025). The rejection however was reduced from 71.3 to just 68.8% in the first half an hour indicating that fundamental pore wetting and main fouling layer formation has commenced but not completed up to 30 min (Al-Alawy et al., 2019; Cai et al., 2023).

SiC-containing membranes (B–E) showed a more stable rejection profile over time than membrane A. In particular, the increase of the B module was gradual and reached maximum 90.20% at 50 min, stabilising at 90.34% until 60 min. This phenomenon may imply the formation of a stable cake layer or secondary membrane on the surface, which enhanced the solute removal efficiency in long-time filtration, which is often mentioned in ceramic membrane systems (Lagdali et al., 2026). SiC might also contribute to mechanical stabilization and the retention of pore structure under hydrodynamic stress (Shi et al., 2023; Yan et al., 2025).

Relatively stable rejection values (86–87%) of membranes C and D at all time points implied consistent pore connectivity and anti-fouling ability. Their results imply that the rejection is governed by pore topology rather than just by size. Solute transport through membranes is controlled by both pore geometry and tortuosity as per the theory of porous media (Onyenanu and Nwabanne, 2025). The lower but steady rejection of C and D suggests a trade-off between permeability and selectivity, which is reasonably useful in the actual filtration process.

Membrane E had good rejection during first 40 min (87–88%) followed by significant drop to 83.15% at 60 min. This decrease might be due not just to possible loss of structural integrity but also to the partial pore-enlargement leading, for instance, to less bulk separation. Comparable reductions in rejection as function of time for high porous ceramic membranes at long hydraulic loading times have been observed elsewhere (Abdulhameed et al., 2023; do Carmo et al., 2024).

Over all, the obtained results of the time-dependent rejection have to be interpreted joining these supporting raw UV–Vis spectra absorbance calculation table and repeated measurements that information on value of rejection was based on experimental filtration test.

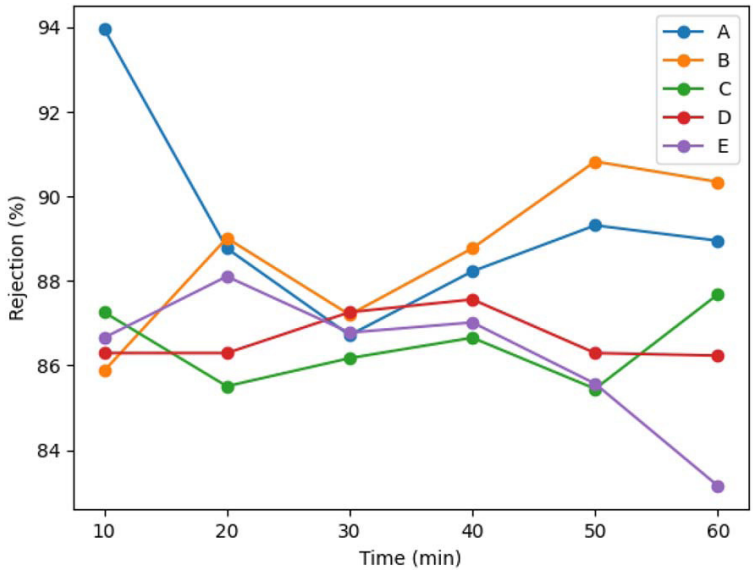

Figure 10. Time-dependent rejection efficiency of ceramic membranes A–E calculated from spectrophotometric absorbance data (A_0 = 1.656)

CONCLUSIONS

Ultraporous Al–Fe pillared bentonite–SiC ceramic membranes can be produced having adjustable structural and mechanical attributes with high filtration properties. It proves that the stable mechanically dual adsorptive-filtration membrane aimed to be developed was successful under the low-temperature sintering condition used. Synergistic effects were observed due to the relationship between Al–Fe pillared bentonite and SiC, as the clay led to pore formation and conferring adsorbent functionality, while SiC reinforced framework stability in addition to antifouling resistance.

Microstructural analysis corroborated that membrane morphology changed substantially as a function of composition, from native clay-rich structures which were originally highly porous but lacked a strong mechanical response to tightly packed and brittle SiC-rich systems. Porosity and pore size of the membranes were previously reported to have open porosity values of 46.83–52.44% with mean pore sizes of 0.12–0.28 µm, hence asserting that the pore system can be adjusted by altering the AFPB/SiC ratio. Midpoint mixtures in the composition of laboratory synthesis, especially when they contained balanced contents of pillared bentonite and SiC, had bicontinuous porous networks that gave greater pore uniformity and better connected porosity. Such a structural configuration led to an appropriate compromise between permeability and mechanical resistance, suggesting that pore structure and phase distribution are more determining factors than total porosity solely.

The results of performance assessment testified that pure pillared bentonite membranes showcased a high initial flux but quickly deteriorated due to extreme fouling, whereas SiC-modified membranes exhibited stable flux as well as resistance against pore blockage. Of the various membranes tested, the flexural strength of the 40:60 Al–Fe pillared bentonite/SiC membrane was found to be highest (28.6 MPa), suggesting that this composition provides significant reinforcement. Among the studied compositions, moderate amounts of SiC in the membranes yielded the most stable membrane permeation behavior, as determined by flux during long-term filtration. In parallel, whilst all membranes achieved high dye rejection, with values remaining above 83%, SiC-containing composites showed increased stability in their rejection profile which is attributable to an improved structural integrity and controlled pore topology during operation.

In general, the results validate the implementation of an adsorption-filtration dual-functionality in Al–Fe pillared bentonite matrices with controllable SiC incorporation. The research bridges the knowledge gap of how Al-Fe pillared bentonite combined to SiC regulates pore evolution, mechanical reinforcement, flux stability and dye rejection in one composite ceramic

membrane system. The resulted composite membranes exhibit excellent permeability, selectivity and mechanical durability, showing feasibility as low-cost and environmental friendly materials for dye-contaminated wastewater. Nonetheless, the 100% SiC membrane was too brittle for reproducible assessment showing that SiC in isolation is not adequate without a clay-based binding matrix at 800 °C and further studies will be needed to include long-term recyclability data, industrially relevant textile wastewater tests, fouling resistance characterisation and additional surface analysis studies.

Acknowledgements

This research was financially supported by Ministry of Higher Education, Science, and Technology of the Republic of Indonesia through National Competitive Research Program, Regular Fundamental Research Scheme (Grant Number: 123/C3/DT.05.00/PL/2025 and 177 /LL2/DT.05.00/PL/2025).

REFERENCES

1. Abdel-Azim, S. M., Aboul-Gheit, N. A. K., Younis, S. A., Ahmed, S. M. (2025). Synergistic role of pillared bentonite with single and binary Fe/Al-polyoxocations on Pb(II) adsorption recovery from hard water under competitive and non-competitive effects. Applied Clay Science, 267(April 2025), 1–7. https://doi.org/10.1016/j.clay.2025.107716
2. Abdulhameed, M. A., Rahman, M. H., Azziz, H. N. (2023). High porous ceramic for oil/water separation: Calcite as a sintering aid. Journal of Ecological Engineering, 24(7), 88–95. https://doi.org/10.12911/22998993/163348
3. Achiou, B., Adlane, S., Harrati, A., Belgada, A., Aaddane, A., Elidrissi, Z. C., Ouammou, M., Sadik, C., Younssi, S. A. (2025). Low-cost ceramic peridotite membrane developed with geomaterial-based sintering aids for textile wastewater treatment. Journal of Environmental Chemical Engineering, 13(3), 116375. https://doi.org/10.1016/j.jece.2025.116375
4. Akash, F. A., Shovon, S. M., Rahman, W., Rahman, M. A., Chakraborty, P., Prasetya, T. A. E., Monir, M. U. (2024). Advancements in ceramic membrane technology for water and wastewater treatment: A comprehensive exploration of current utilizations and prospective horizons. Desalination and Water Treatment, 319, 100569. https://doi.org/10.58532/v3bars2p2ch2
5. Akoumeh, R., Al-Ejji, M., Aljaoni, B., Abbas, M. (2025). Advances in ceramic membrane technology: Versatility of fabrication technique, industrial applications, and challenges. Inorganic Chemistry Communications, 179, 2025–2027. https://doi.org/10.1016/j.inoche.2025.114685
6. Al-Alawy, R. M. J., Abod, B. M., Kamar, F. H., Nechifor, A. C. (2019). Removal of dyes from wastewater by ceramic membrane. Revista de Chimie, 70(5), 1715–1719. https://doi.org/10.37358/rc.19.5.7200
7. Bahrouni, J., Attia, A., Elberrichi, F. Z., Baklouti, L. (2025). Green and sustainable clay ceramic membrane preparation and application to textile wastewater treatment for color removal. Membranes, 15(292). https://doi.org/10.3390/membranes15100292
8. Biswas, B., Majumder, C. (2026). Electrochemical remediation of reactive Red 141 Dye using clay-based ceramic membranes: Performance evaluation and degradation pathway analysis. Journal of Environmental Chemical Engineering, 14(1), 1–7. https://doi.org/10.1016/j.jece.2025.120937
9. Boutaleb, M., Tabit, K., Mansori, M., Saadi, L., Waqif, M. (2025). Facile and low-cost method for preparing multilayer ceramic membranes based on cordierite and abundant clay: Application to dye removal. Separation and Purification Technology, 362(July 2025), 1–6. https://doi.org/10.1016/j.seppur.2025.131752
10. Boutaleb, M., Tabit, K., Mansori, M., Saâdi, L., Waqif, M. (2024). Development of low-cost clayey ceramic filtering membrane with controllable porosity and high mechanical strength. Ceramics International, 50(18), 32771–32782. https://doi.org/10.1016/j.ceramint.2024.06.087
11. Cai, C., Sun, W., He, S., Zhang, Y., Wang, X. (2023). Ceramic membrane fouling mechanisms and control for water treatment. Frontiers of Environmental Science and Engineering, 17(10), 1–18. https://doi.org/10.1007/s11783-023-1726-9
12. Chen, M., Heijman, S. G. J., Luiten-Olieman, M. W. J., Rietveld, L. C. (2022). Oil-in-water emulsion separation: Fouling of alumina membranes with and without a silicon carbide deposition in constant flux filtration mode. Water Research, 216(March). https://doi.org/10.1016/j.watres.2022.118267
13. Chihi, R., Comite, A., Mansour, L., Ayari, F. (2024). Microstructural evolution and physico-chemical properties of a synthesized series of porous ferric and bentonite ceramic membranes. Ceramics International, 50(5), 7355–7365. https://doi.org/10.1016/j.ceramint.2023.11.379
14. Das, D., Kayal, N., Innocentini, M. D. de M. (2021). Permeability behavior and wastewater filtration performance of mullite bonded porous sic ceramic

membrane prepared using coal fly ash as sintering additive. Transactions of the Indian Ceramic Society, 80(3), 186–192. https://doi.org/10.1080/0371750X.2021.1934122

15. Desai, H., A, K., Reddy, G. S. K. (2023). Sustainable and rapid pillared clay synthesis with applications in removal of anionic and cationic dyes. Microporous and Mesoporous Materials, 352(March 2023), 1–9. https://doi.org/10.1016/j.micromeso.2023.112488
16. do Carmo, E. S., Silva, W. L., dos Santos Barbosa, A., Rodrigues, M. G. F. (2024). Low-cost ceramic membrane production for dye removal. Desalination and Water Treatment, 320(October). https://doi.org/10.1016/j.dwt.2024.100726
17. El-shazly, A. H., Fahmy, Y. A. (2025). Cost-effective and durable ceramic membrane : fabrication and performance optimization. Membranes, 15(307), 1–18. https://doi.org/10.3390/membranes15100307
18. El Abbadi, S., El Moustansiri, H., Douma, M., Bouazizi, A., Baidou, M., Elgamouz, A., Tijani, N. (2025). Effective elimination of Congo red dye from tannery wastewater using Fe-pillared bentonite: Synthesis, adsorption isotherm, kinetics, and optimization via Box-Behnken design. Microporous and Mesoporous Materials, 392, 1–6. https://doi.org/10.1016/j.micromeso.2025.113641
19. Foorginezhad, S., Rezvannasab, G., Asadnia, M. (2023). Natural clay membranes: A sustainable and affordable solution for treating dye solutions, coal mine washery waste, and aquaculture wastewater. Journal of Water Process Engineering, 54(March). https://doi.org/10.1016/j.jwpe.2023.104012
20. Fu, Q., Ma, Y., Wang, J., Yang, Y., Wang, P., Li, S., Zhao, Y. (2024). Digital light processing of high-purity SiC ceramic membrane support modified by SiC whisker. Ceramics International, 50(21), 41237–41245. https://doi.org/10.1016/j.ceramint.2024.07.435
21. Fu, Z., Zhang, L., Chen, C., Yang, S., Xu, R., Fu, X., Zhu, L., Shi, H., Xu, M. (2025). High porosity and robust strength silicon carbide ceramic membrane for water treatment. Journal of the European Ceramic Society, 45(13), 4–9. https://doi.org/10.1016/j.jeurceramsoc.2025.117478
22. Fu, Z., Zhou, Z., Liu, Z., Yang, H., Chen, Z. (2024). Feasibility and challenges of low-cost ceramic membranes in water treatment applications. Desalination and Water Treatment Journal, 320(August). https://doi.org/https://doi.org/10.1016/j.dwt.2024.100739
23. Ghohestani, E., Samari, F., Yousefinejad, S. (2022). An efficient removal of methylene blue and lead (II) from aqueous solutions by green synthesized iron oxide / pillared bentonite nanocomposite. Materials Chemistry and Physics, 287(August 2022), 1–8. https://doi.org/10.1016/j.matchemphys.2022.126266
24. Hamad, K. H., Abdallah, H., Aly, S. T., Abobeah, R., Amin, S. K. (2024). Fabrication and assessment of performance of clay based ceramic membranes impregnated with CNTs in dye removal. Scientific Reports, 14(1). https://doi.org/10.1038/s41598-024-77015-3
25. Hotza, D., Di Luccio, M., Wilhelm, M., Iwamoto, Y., Bernard, S., Diniz da Costa, J. C. (2020). Silicon carbide filters and porous membranes: A review of processing, properties, performance and application. Journal of Membrane Science, 610. https://doi.org/10.1016/j.memsci.2020.118193
26. Huang, X., Deng, P., Chen, W., Hu, X. (2023). Low-temperature sintering of porous SiC ceramic membrane with industrial-grade sodium meta-aluminate as a sintering additive. Ceramics International, 49(23), 39090–39098. https://doi.org/10.1016/j.ceramint.2023.09.248
27. Jang, H., Kang, S., Kim, J. (2024). Identification of membrane fouling with greywater filtration by porous membranes: combined effect of membrane pore size and applied pressure. Membranes, 14(2). https://doi.org/10.3390/membranes14020046
28. Jarrar, R., Abbas, M. K. G., Al-Ejji, M. (2024). Environmental remediation and the efficacy of ceramic membranes in wastewater treatment—a review. Emergent Materials, 7(4), 1295–1327. https://doi.org/10.1007/s42247-024-00687-0
29. Kanth, M. S., Sandhya Rani, S. L., Raja, V. K. (2025). Advancing ceramic membrane technology in chemical industries applications by evaluating cost-effective materials, fabrication and surface modification methods. Hybrid Advances, 8(January). https://doi.org/10.1016/j.hybadv.2025.100380
30. Ke, X., Zhang, J., Jin, Q., Ni, Y., Wang, J., Wu, H. (2025). Modulation of pore structure in SiC porous ceramics: Impact of SiC powder particle size and distribution span. Materials Chemistry and Physics, 334(April 2025), 1–7. https://doi.org/10.1016/j.matchemphys.2025.130504
31. Khmiri, Y., Attia, A., Aloulou, H., Dammak, L., Baklouti, L., Ben Amar, R. (2023). Preparation and characterization of new and low-cost ceramic flat membranes based on zeolite-clay for the removal of indigo blue dye molecules. Membranes, 13(11). https://doi.org/10.3390/membranes13110865
32. Lagdali, S., El-Habacha, M., Benjelloun, M., Lasfar, M., Mahmoudy, G., Dabagh, A., Miyah, Y., Iaich, S., & Zerbet, M. (2026). Low-cost ceramic membranes: Manufacturing methods, cost analysis and application in water and wastewater treatment: A review. ChemPhysMater, 5, 22–49. https://doi.org/10.1016/j.chphma.2025.08.002
33. Li, J., Gu, Q., Zhang, H., Zhong, Z., Fan, Y., Xing, W. (2025). Electrostatically assembled core-shell particles and their reaction sintering for SiC

membranes with improved oil / water separation and thermal regeneration ef fi ciency. Advanced Membranes, 5(April), 100148. https://doi.org/10.1016/j.advmem.2025.100148

34. Liang, Z., Zhang, H., Li, Y., Zhang, W., Zhou, J., Gu, Q., Zhong, Z., Xing, W. (2024). A reverse particle grading strategy for design and fabrication of porous SiC ceramic supports with improved strength. Journal of Advanced Ceramics, 13(7), 1011–1022. https://doi.org/10.26599/JAC.2024.9220915
35. Liu, B., Wang, Z., Tan, X., Liu, S. (2024). Ultra-high flux ceramic hollow fiber membranes for nanofiltration. Journal of Membrane Science, 709(September 2024), 1–7. https://doi.org/10.1016/j.memsci.2024.123104
36. Malebadi, K. A., Sawunyama, L., Seheri, N. H., Onwudiwe, D. C. (2025). Application of ceramic membranes derived from waste and natural materials for the removal of organic dyes from wastewater: A review. Ceramics, 8(3), 80. https://doi.org/10.3390/ceramics8030080
37. Marques, A. V. S., Barbosa, A. dos S., Maia, L. F., Rodrigues, M. G. F., Lins Almeida Barbosa, T., Luna, C. B. B. (2025). Development and characterization of sawdust-based ceramic membranes for textile effluent treatment. Membranes, 15(10), 1–28. https://doi.org/10.3390/membranes15100298
38. Onyenanu, C. N., Nwabanne, J. T. (2025). Application of ceramic membranes for the removal of heavy metals and dyes: Efficiency and performance review. Research Journal in Civil, Industrial and Mechanical Engineering, 2(2), 84–98. https://doi.org/10.61424/rjcime.v2i2.338
39. Parodia, A., Prasniski, J. A., Bertella, F., Pergher, S. B. C. (2021). Keggin-al13 polycations: Influence of synthesis and intercalation parameters on the structural properties of al-pillared clays. Minerals, 11(11). https://doi.org/10.3390/min11111211
40. Rakcho, Y., Baidou, M., Naboulsi, A., Bouazizi, A., Mouiya, M., Abouliatim, Y., Benhammou, A., Ouammou, M., Abourriche, A., Alami, J. (2025). Fabrication of low-cost ceramic nanofiltration membrane from natural resources for the removal of cationic and anionic dyes : Experimental and DFT investigations. Chemical Engineering Journal, 505(February), 1–8. https://doi.org/10.1016/j.cej.2025.159779
41. Rakcho, Y., Mouiya, M., Bouazizi, A., Abouliatim, Y., Sehaqui, H., Benhammou, A., Mansouri, S., Hannache, H., Alami, J., Abourriche, A. (2024). Enhanced mechanical strength of micro-porous ceramics through the removal of alkaline earth carbonates from Moroccan red clay for membrane support application. Arabian Journal of Chemistry, 17(1). https://doi.org/10.1016/j.arabjc.2023.105484
42. Rakcho, Y., Naboulsi, A., Mansouri, S., Mouiya, M., Sehaqui, H., Bouazizi, A., Abouliatim, Y., Benhammou, A., Abourriche, A., Alami, J. (2024). Sustainable valorization of food waste into a pore-forming agent for ceramic membrane production: Experimental and DFT studies on methylene blue dye removal. Sustainable Materials and Technologies, 42(December 2024), 1–8. https://doi.org/10.1016/j.susmat.2024.e01181
43. Ramteke, P. K., Rathod, A. P., Kodape, S. M., Sonawane, S. S. (2025). Development and evaluation of environmentally sustainable cenosphere ceramic membrane for the efficient separation of methylene blue dye. Chemical Papers, 79(1), 313–332. https://doi.org/10.1007/s11696-024-03782-y
44. Rezala, H., Douba, H., Boukhatem, H., Romero, A., El, R. D. T. (2020). Adsorption of methylene blue by hydroxyl-aluminum pillared montmorillonite. J.Chem.Soc.Pak., 42(04), 550–563.
45. Riyanti, F., Hariani, P. L., Hasanudin, H., Rachmat, A. (2024). Optimization photodegradation of methylene blue dye using bentonite / PDA / Fe_3O_4 @ CuO Composite by Response Surface Methodology. Bulletin of Chemical Reaction Engineering & Catalysis, 19(2), 252–264. https://doi.org/10.9767/bcrec.20132
46. Roy, S. (2025). Properties and advanced applications of porous ceramic composites. Open Ceramics, 21(November 2024). https://doi.org/DOI: 10.1016/j.oceram.2024.100714
47. Saja, S., Bouazizi, A., Achiou, B., Ouaddari, H., Karim, A., Ouammou, M., Aaddane, A., Bennazha, J., Alami Younssi, S. (2020). Fabrication of low-cost ceramic ultrafiltration membrane made from bentonite clay and its application for soluble dyes removal. Journal of the European Ceramic Society, 40(6), 2453–2462. https://doi.org/10.1016/j.jeurceramsoc.2020.01.057
48. Satyannarayana, K. V. V., Rani, S. L. S., Baranidharan, S., Kumar, R. V. (2022). Indigenous bentonite based tubular ceramic microfiltration membrane: Elaboration, characterization , and evaluation of environmental impacts using life cycle techniques. Ceramics International, 48(19), 1–7. https://doi.org/10.1016/j.ceramint.2022.03.156
49. Sheng, D., Wang, T., Zhang, Y., Sun, M., Liu, R., Zhang, X., Liu, H., Qu, J. (2025). Reconstruction and analysis of pore blockage fouling in ceramic ultrafiltration membranes through FIB-SEM. Nature Communications. https://doi.org/10.1038/s41467-025-67662-z
50. Shi, S., Jian, K., Fang, M., Guo, J., Rao, P., Li, G. (2023). SiO2 Modification of silicon carbide membrane via an interfacial in situ sol–gel process for improved filtration performance. Membranes, 13(9). https://doi.org/10.3390/membranes13090756
51. Wang, J., Sui, S., Fu, Q., Yang, Y., Fu, J., Meng, F., Li, S. (2024). Pure-SiC ceramic membrane for

ultrafiltration: Morphology, pore characteristics and separation performances. Ceramics International, 50(5), 8162–8170. https://doi.org/10.1016/j.ceramint.2023.12.146

52. Wang, Y., Ma, B., Ulbricht, M., Dong, Y. (2022). Progress in alumina ceramic membranes for water purification : Status and prospects. 226(November 2022), 1–8. https://doi.org/10.1016/j.watres.2022.119173
53. Wei, W., Li, Q., Zhou, G., Zeng, Y., Han, F. (2025). One-step sintering of three gradient hierarchical SiC ceramic membrane with high flux for ultrafine particle filtration. Journal of Membrane Science, 734(October 2025), 124473. https://doi.org/10.1016/j.memsci.2025.124473
54. Xie, Y., Fang, Y., Chen, D., Wei, J., Fan, C., Zhu, X., Liu, H. (2025). Membrane fouling control and treatment performance using coagulation–tubular ceramic membrane with concentrate recycling. Membranes, 15(8), 225. https://doi.org/10.3390/membranes15080225
55. Xue, R., Yu, T., Song, H., Sun, Y., Deng, X. (2023). Effect of SiO_2 adding on properties of SiC porous ceramic support. Journal of Physics: Conference Series, 2468(1). https://doi.org/10.1088/1742-6596/2468/1/012009
56. Yan, B., Chen, Z., Wang, Y., Liu, J., Wang, R., Li, X., Fang, M., Li, G., Rao, P., Liu, Y. (2025). Pore size engineering of SiC ceramic membrane with pre-ceramic polymer for high retention performance and corrosion resistance. Ceramics International, 51(29), 60844–60854. https://doi.org/10.1016/j.ceramint.2025.10.279
57. Yan, P., Pu, Z., Du, M., Ge, X., Dong, J., Wang, H., Li, J., Cui, Z. (2025). Preparation of ceramic membranes with small pore size, narrow pore size distribution and investigation of oil-water separation mechanism. Journal of Membrane Science, 716(February 2025), 1–8. https://doi.org/10.1016/j.memsci.2024.123522
58. Yang, J., Zhang, X., Zhang, B., Liu, F., Li, W., Jian, J., Zhang, S., Yang, J. (2022). Mullite ceramic foams with tunable pores from dual-phase sol nanoparticle-stabilized foams. Journal of the European Ceramic Society, 42(4), 1703–1711. https://doi.org/10.1016/j.jeurceramsoc.2021.12.008
59. Zhang, Y., Han, F., Zou, D. (2025). Fabrication of high-performance SiC ceramic membranes modified using in situ grown mullite whiskers and high-temperature filtration. Separation and Purification Technology, 358(June 2025), 1–6. https://doi.org/10.1016/j.seppur.2024.130328
60. Zhu, L., Wang, W., Zhao, P., Wang, S., Yang, K., Shi, H., Xu, M., Dong, Y. (2022). Silicon carbide catalytic ceramic membranes with nano-wire structure for enhanced anti-fouling performance. Water Research, 226. https://doi.org/10.1016/j.watres.2022.119209